Article

Conformational Substates Modulate Hydride Transfer in Dihydrofolate Reductase

Ian F. Thorpe, and Charles L. Brooks

J. Am. Chem. Soc., **2005**, 127 (37), 12997-13006• DOI: 10.1021/ja053558l • Publication Date (Web): 25 August 2005

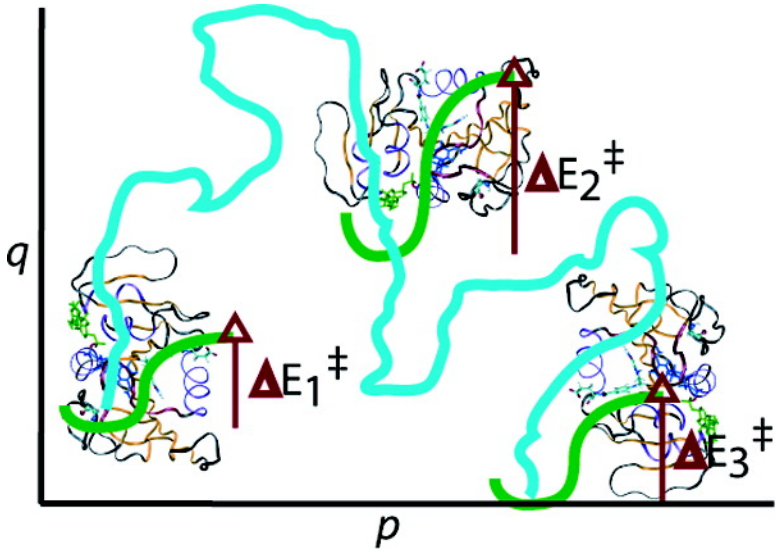

More About This Article

Additional resources and features associated with this article are available within the HTML version:

- Supporting Information
- Links to the 11 articles that cite this article, as of the time of this article download
- Access to high resolution figures
- Links to articles and content related to this article
- Copyright permission to reproduce figures and/or text from this article

View the Full Text HTML

J|A|C|S
ARTICLES
Published on Web 08/25/2005

Conformational Substates Modulate Hydride Transfer in Dihydrofolate Reductase

Ian F. Thorpe and Charles L. Brooks III*

Contribution from the Department of Molecular Biology, The Scripps Research Institute, 10550 North Torrey Pines Road, La Jolla, California 92037

Received May 31, 2005; E-mail: brooks@scripps.edu

Abstract: In earlier studies of the hydride-transfer reaction catalyzed by dihydrofolate reductase (DHFR) we identified features of the protein correlated with variations in the reaction barrier. We extend the scope of those studies by carrying out potential of mean force (PMF) simulations to determine the hydride-transfer barrier in the wild-type protein as well as the G121V and G121S mutants. While our prior studies focused on the reactant state, our current work addresses the full reaction pathway and directly probes the reactive event. The free energy barriers and structural ensembles resulting from these PMF calculations exhibit the same trends reported in our previous work. Fluctuations present in these simulations also exhibit trends associated with differences in the hydride-transfer barrier height. Moreover, vibrational modes anticipated to promote hydride transfer exhibit larger amplitudes in simulations that generate lowered barriers. The results of our study indicate that discrete basins (substates) on a potential energy landscape of the enzyme give rise to distinct hydride-transfer barriers. We suggest that the long-range effects of mutations at position 121 within DHFR are mediated by differentially preorganized protein environments in the context of distinct substate distributions, with concomitant changes to the dynamic properties of the enzyme.

1. Introduction

The wealth of information available for the enzyme dihydrofolate reductase (DHFR) has made this protein an attractive model system with which to probe the relationship between protein structure, dynamics, and catalysis. Consequently, it has been extensively studied; for a recent review the reader is directed to Schnell et al.[1] *Escherichia coli* DHFR is a 159-residue protein consisting of a central eight-stranded β-sheet and four α-helices (Figure 1). The active-site cleft within the enzyme is surrounded by three loops on the ligand binding face. These loops are termed Met20 (M20, residues 9−24), βF-βG (residues 116−132), and βG-βH (residues 142−150). DHFR catalyzes the reduction of 7,8-dihydrofolate (DHF) into 5,6,7,8-tetrahydrofolate (THF), a ubiquitous metabolic precursor (Figure 1).

The DHFR reaction mechanism has been characterized via experimental and theoretical approaches.[3−8] The reduction is generally thought to proceed via protonation followed by transfer of a hydride species from the cofactor NADPH to DHF^+ within the active-site cleft of the enzyme. Of particular interest to those who study this enzyme has been the impact of mutations away from the site of chemistry on the hydride-transfer barrier.[9] In particular, changing glycine 121 to valine (G121V) or serine (G121S) is associated with reductions in the hydride-transfer rate despite this residue being more than 15 Å from the site of hydride transfer.[10,11] Theoretical studies of the system suggested that correlated motions within the enzyme are associated with hydride-transfer proficiency.[12−14] Other work identified a network of coupled motions thought to be associated with the hydride-transfer event[15,16] and characterized the electronic stabilization of the reaction by the wild-type[17,18] and G121V[19] proteins.

Our own studies indicated that structural properties of the wild-type, G121V, and G121S proteins are associated with lowered hydride-transfer barriers.[20,21] In contrast to suggesting

(1) Schnell, J. R.; Dyson, H. J.; Wright, P. E. *Annu. Rev. Biophys. Biomol. Struct.* **2004**, *33*, 119−140.
(2) Humphrey, W.; Dalke, A.; Schulten, K. *J. Mol. Graphics* **1996**, *14*, 33−38, 27−28.
(3) Fierke, C. A.; Johnson, K. A.; Benkovic, S. J. *Biochemistry* **1987**, *26*, 4085−4092.
(4) Chen, Y.-Q.; Kraut, J.; Blakley, R. L.; Callender, R. *Biochemistry* **1994**, *33*, 7021−7026.
(5) Bliznyuk, A. A.; Gready, J. E. *J. Comput. Aided Mol. Des.* **1998**, *12*, 325−333.
(6) Cummins, P. L.; Gready, J. E. *J. Am. Chem. Soc.* **2001**, *123*, 3418−3428.
(7) Ferrer, S.; Silla, E.; Tunon, I.; Martí, S.; Moliner, V. *J. Phys. Chem. B* **2003**, *107*, 14036−14041.
(8) Rod, T. H.; Brooks, C. L., III. *J. Am. Chem. Soc.* **2003**, *125*, 8718−8719.
(9) Wagner, C. R.; Huang, Z.; Benkovic, S. J. *Biochemistry* **1994**, *33*, 11576−11585.
(10) Cameron, C. E.; Benkovic, S. J. *Biochemistry* **1997**, *36*, 15792−15800.
(11) Rajagopalan, P. T. R.; Lutz, S.; Benkovic, S. J. *Biochemistry* **2002**, *41*, 12618−12628.
(12) Radkiewicz, J. L.; Brooks, C. L. *J. Am. Chem. Soc.* **2000**, *122*, 225−231.
(13) Rod, T. H.; Radkiewicz, J. L.; Brooks, C. L., III. *Proc. Natl. Acad. Sci. U.S.A.* **2003**, *100*, 6980−6985.
(14) Wong, K. F.; Watney, J. B.; Hammes-Schiffer, S. *J. Phys. Chem. B* **2004**, *108*, 12231−12241.
(15) Agarwal, P. K.; Billeter, S. R.; Rajagopalan, P. T. R.; Benkovic, S. J.; Hammes-Schiffer, S. *Proc. Natl. Acad. Sci. U.S.A.* **2002**, *99*, 2794−2799.
(16) Agarwal, P. K.; Billeter, S. R.; Hammes-Schiffer, S. *J. Phys. Chem. B* **2002**, *106*, 3283−3293.
(17) Garcia-Viloca, M.; Truhlar, D. G.; Gao, J. *J. Mol. Biol.* **2003**, *327*, 549−560.
(18) Garcia-Viloca, M.; Truhlar, D. G.; Gao, J. *Biochemistry* **2003**, *42*, 13558−13575.
(19) Watney, J. B.; Agarwal, P. K.; Hammes-Schiffer, S. *J. Am. Chem. Soc.* **2003**, *125*, 3745−3750.

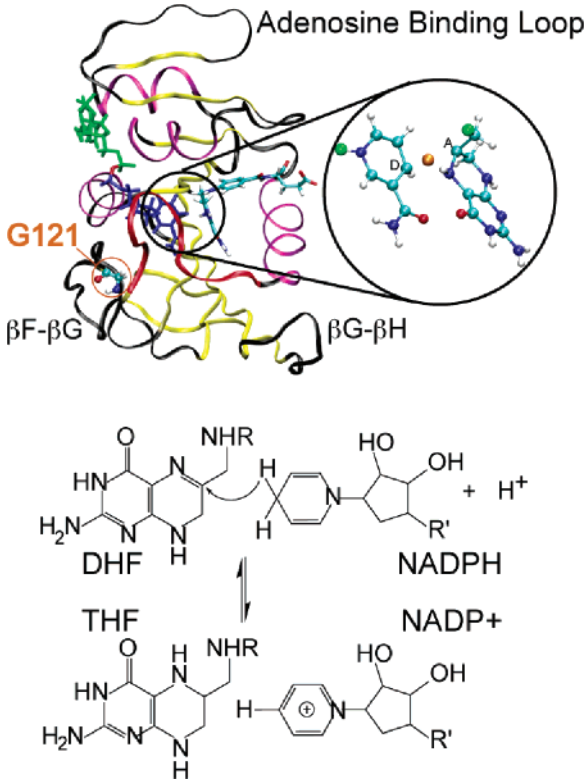

Figure 1. Ribbon representation of DHFR, color-coded to display elements of secondary structure. Yellow, purple, and black represent β-strand, α-helix, and coil/loop regions, respectively. The M20 loop is displayed in red; other loops within the enzyme as well as the position of glycine 121 are labeled. DHF (right) and NADPH (left) within the active site are shown in tube representation. The asterisk denotes NADPH atom C3 referred to in section 2.5. The inset displays the quantum mechanical region employed for our calculations. Green spheres within this region are GHO boundary atoms (see Methods), while the orange sphere is the transferred hydride. The donor and acceptor carbons are labeled D and A, respectively. Illustrations were generated using the VMD program.[2] The panel below depicts the chemical transformation that accompanies hydride transfer.

that dynamics are important for the effects of these mutations to be mediated, our findings suggested that static, equilibrium distributions of protein conformations were sufficient to account for the rate-diminishing effects of mutations at position 121. In particular, these mutations act to disrupt the equilibrium distributions of the M20 loop which abuts the site of chemistry in the enzyme (see Figure 1). This loop has been shown to play an important role in catalysis,[22] and conformational changes of this loop occur throughout the DHFR catalytic cycle.[23]

Complex systems such as proteins are characterized by high-dimensional energy landscapes that encompass numerous local energy minima.[24] Conformational changes such as those observed for the M20 loop in DHFR involve transitions between these minima. We refer to these energy minima as substates, a term introduced by Frauenfelder and colleagues.[25] The evolution of a protein trajectory can thus be thought of as motion between substates in this high-dimensional space. We assert that these substates must be accounted for when functional properties of proteins are considered and provide evidence for their role in modulating catalytic efficacy in DHFR.

A limitation of our earlier studies was that they focused on properties of the reactant states only, with the assumption that the corresponding transition states reflect a slight perturbation of the reactant-state configurations. While there are many indications that this is a reasonable approach, this assumption was not explicitly tested. We have addressed this concern by using combined quantum mechanical/molecular mechanical (QM/MM) methods to generate potentials of mean force (PMFs) associated with the hydride transfer. These simulations allow us to identify structural and dynamic features that directly impact the hydride-transfer barrier in the enzyme. The hydride-transfer barrier was previously characterized for a number of molecular dynamics (MD) snapshots by carrying out minimum energy path (MEP) calculations.[20] For each of the wild-type, G121S, and G121V enzymes, we employed two different initial conditions to generate PMFs. One simulation was begun from a snapshot that produced a low barrier to hydride transfer as a result of the prior MEP calculations and the other from a snapshot that produced a high MEP barrier.

The structural features of the protein found to be correlated with modulations in the barrier height in our earlier work[21] did not change significantly during the course of the PMF simulations. In addition, the energy barriers resulting from the PMF simulations display trends similar to those present in the original MEP calculations. Thus, the conformational substates that influence the MEP calculations are sufficiently long-lived to influence the PMFs. By extension, the patterns of interaction associated with these substates are likely to have similar roles in modulating the reactive event in both sets of calculations.

Furthermore, we demonstrate that these changes occur in concert with modifications to DHFR dynamics. The PMF simulations were employed to characterize fluctuations that occur in substates giving rise to heightened or lowered hydride-transfer barriers. Correlated fluctuations were found to differ between the two classes of substates as well as among the mutant and wild-type proteins. Vibrational modes expected to facilitate hydride transfer and entropic measures computed for each simulation exhibited similar differences.

2. Methods

2.1. QM/MM Simulations. In our previous studies, we employed MEP calculations to characterize ensembles of hydride-transfer barrier for the wild-type, G121V, and G121S DHFR proteins.[20] Snapshots were selected from the original MD simulations that generated these ensembles to become the initial conditions for our PMF simulations. The original MD simulations were based on the 1rx2 crystallographic coordinates of the wild-type protein[26] and were carried out for the Michaelis complex DHFR:DHF:NADPH in each enzyme. Details of this work have been published elsewhere.[12,13] For each protein we selected a snapshot that had exhibited the highest barrier via the MEP calculations and one that had exhibited the lowest barrier for each of the wild-type, G121V, and G121S proteins. These will be referred to as WTHI, WTLO, GVHI, GVLO, GSHI and GSLO, respectively. Using coordinates from these simulations, we generated a 30-Å sphere of TIP3P[27] solvent around each protein centered on the position of the

(20) Thorpe, I. F.; Brooks, C. L., III. *J. Phys. Chem. B* **2003**, *107*, 14042−14051.
(21) Thorpe, I. F.; Brooks, C. L., III. *Proteins* **2004**, *57*, 444−457.
(22) Li, L.; Falzone, C. J.; Wright, P. E.; Benkovic, S. J. *Biochemistry* **1992**, *31*, 7826−7833.
(23) Venkitakrishnan, R. P.; Zaborowski, E.; McElheny, D.; Benkovic, S. J.; Dyson, H. J.; Wright, P. E. *Biochemistry* **2004**, *43*, 16046−16055.
(24) Elber, R.; Karplus, M. *Science* **1987**, *235*, 318−321.
(25) Frauenfelder, H.; Sligar, S. G.; Wolynes, P. G. *Science* **1991**, *254*, 1598−1603.
(26) Sawaya, M. R.; Kraut, J. *Biochemistry* **1997**, *36*, 586−603.
(27) Jorgensen, W. L.; Chandrasekhar, J.; Madura, J. D.; Impey, R. W.; Klein, M. L. *J. Chem. Phys.* **1983**, *79*, 926−935.

transferred hydrogen. The integrity of the solvent sphere was maintained through the use of a stochastic boundary potential.[28]

The DHF pteridine ring was protonated at position N5 to generate the ternary reactive complex DHFR:DHF^+:NADPH. We employed a combined quantum mechanical/molecular mechanical (QM/MM) approach to simulate the reactive event. The QM treatment was provided by the PM3 semiempirical method, while the MM component was provided by the standard CHARMM 22 force field.[29] Regions within the nicotinamide headgroup and DHF pteridine ring were designated QM atoms as displayed in Figure 1. The generalized hybrid orbital link atom method was employed to connect the QM and MM regions.[30] This QM/MM interface is the same as that reported in our previous work.[20] Simulations were carried out with the CHARMM molecular mechanics program.[29] With the initial protein configurations from the MD snapshots held fixed, the energy of DHF, NADPH, and solvent within 10 Å of the QM atoms was minimized using the adobted basis Newton−Raphson method until a tolerance of 0.001 kcal/mol·Å on the gradient was achieved. During this process, a large restraint was applied to enforce the desired value of the hydride-transfer reaction coordinate. All restraints were then removed and umbrella potentials added to facilitate sampling along the reaction coordinate (see below). Molecular dynamics simulations were carried out in the canonical (NVT) ensemble at 298 K using a Nosé−Hoover thermostat. A time step of 1 fs was employed, and the equations of motion were integrated with the velocity Verlet scheme. Coordinates were saved every 25 steps. All bond distances between hydrogen and heavy atoms were constrained with the SHAKE algorithm[31] except for those atoms in the QM region.

2.2. PMF Generation. To generate a PMF for the hydride transfer we employed an umbrella sampling approach. A reaction coordinate λ was chosen to represent different stages of the hydride-transfer process. The value of λ is given by the difference between the donor−hydride and acceptor−hydride distances:

$$\lambda = r_{AH} - r_{DH} \tag{1}$$

where r_{AH} is the acceptor−hydride distance and r_{DH} is the donor−hydride distance. Comparable reaction coordinates have been employed in the study of similar hydride-transfer reactions.[32] Note that this coordinate is the negative of that employed by Garcia-Viloca et al. in their study of DHFR.[18] Umbrella potentials U_i, of the form

$$U_i = \frac{k}{2}(\lambda_{o,i} - \lambda)^2 \tag{2}$$

were employed for each simulation window i. The force constant k varied from 100 to 350 kcal/mol·Å^2, depending on position along the reaction coordinate. By employing different target $\lambda_{o,i}$ values, the transferred hydrogen was made to sample different values of the reaction coordinate during conversion from reactants to products.

Two sets of simulations were carried out. In the first set, rather large force constants were employed to obtain an estimate of the hydride-transfer barrier. Based on this approximate free energy barrier, an umbrella potential, U_{PMF}, was constructed that was roughly the negative of this PMF:

$$U_{PMF} = -\frac{1}{2}(17.5 - \zeta)^2$$
$$\zeta = r_{DH}^2 + r_{AH}^2 \tag{3}$$

Table 1. Parameters for U_{SVB} Potential

	D_i (kcal/mol)	α (Å^{-1})	r_i^o (Å)	V_{12} (kcal/mol)
r_{DH}	214.1	0.5	1.11	23.0
r_{AH}	245.7	0.4	1.10	

Further simulations were carried out subject to this potential in addition to individual harmonic potentials U_i (eq 2) along the reaction coordinate. Employing two umbrella potentials in this manner enabled us to use much smaller force constants in each window, facilitating characterization of the underlying free energy surface. Moreover, this approach made convergence of the weighted histogram analysis method (WHAM[33,34]) more efficient by creating more overlap between successive simulation windows. After the simulations were completed, the probability distribution along λ was collected and binned in 0.01-Å increments. The final PMF curves were generated with data from both sets of simulations by applying WHAM along both λ and ξ dimensions. Values of $\lambda_{o,i}$ ranged from −1.6 to 1.6 Å during the simulations, while ξ ranged from 10 to 2.4 Å^2. Spacing between windows was based on $\lambda_{o,i}$ values and varied from 0.2 Å in the vicinity of the reactant or product states to 0.1 Å near the transition state ($\lambda \approx 0$). Depending on the particular simulation, the number of windows employed ranged from 30 to 20. Sampling for each window was continued until convergence of the PMF was achieved. This generally required ∼200 ps of sampling for each of the product or reactant windows and ∼400 ps for windows in the transition-state region.

This approach is similar to that employed by Garcia-Viloca et al.[18] In addition to the QM/MM potential described above, these authors employed a simple valence bond (SVB) term, U_{SVB}, to correct for the overestimation of the gas-phase hydride-transfer barrier by the AM1 semiempirical method used in those studies. The form of this term is given by

$$U_{SVB} = \frac{1}{2}[M_1(r_{DH}) + M_2(r_{AH}) - \sqrt{(M_2(r_{AH}) - M_1(r_{DH}))^2 + 4V_{12}^2}] + D_1 \tag{4}$$

where $M_i(r_i)$ is a Morse potential:

$$M_i(r_i) = D_i[e^{-2\alpha(r_i - r_i^o)} - 2\, e^{-\alpha(r_i - r_i^o)}] \tag{5}$$

The parameters employed in these expressions are presented in Table 1. Note that the original definition presented by these authors contained a typographical error, in that the parameters for the donor−hydride and acceptor−hydride distances were interchanged (Jiali Gao, personal communication). The AM1 and PM3 approaches are very similar, so it is reasonable to apply the SVB correction to our PM3 QM/MM simulations. After carrying out simulations with the bare QM/MM potential, we took this SVB term into account by adding it to our data as an *a posteriori* correction during WHAM. While some error will be introduced by carrying out this procedure, the resulting PMF curves should approximate those generated from simulations that include the SVB term.

2.3. Clustering Analysis. Backbone ϕ/ψ angles for specific residues were recorded and grouped using the ART-2 clustering algorithm implemented in CHARMM.[35] ART-2 is an optimal clustering algorithm based on a self-organizing neural net. The algorithm incorporates an iterative minimization procedure to minimize the Euclidian distance

(28) Brooks, C. L.; Karplus, M. *J. Chem. Phys.* **1983**, *79*, 6312−6325.
(29) MacKerell, A. D., Jr.; Brooks, B.; Brooks, C. L., III; Nilsson, L.; Roux, B.; Won, Y.; Karplus, M. In *The Encyclopedia of Computational Chemistry*; Schleyer, P. v. R., Ed.; John Wiley and Sons: Chichester, 1998; Vol. 1, pp 271−277.
(30) Gao, J.; Amara, P.; Alhambra, C.; Field, M. J. *J. Phys. Chem. A* **1998**, *102*, 4714−4721.
(31) Ryckaert, J. P.; Ciccotti, G.; Berendsen, H. J. C. *J. Comput. Phys.* **1977**, *23*, 327−341.
(32) Alhambra, C.; Corchado, J. C.; Sanchez, M. L.; Gao, J.; Truhlar, D. G. *J. Am. Chem. Soc.* **2000**, *122*, 8197−8203.
(33) Kumar, S.; Bouzida, D.; Swendsen, R. H.; Kollman, P. A.; Rosenberg, J. M. *J. Comput. Chem.* **1992**, *13*, 1011−1021.
(34) Roux, B. *Comput. Phys. Commun.* **1995**, *91*, 275−282.
(35) Karpen, M. E.; Tobias, D. J.; Brooks, C. L., III. *Biochemistry* **1993**, *32*, 412−420.

between a cluster center and its members. Various combinations of the simulation data were employed in order to assess differences between the dihedral distributions. In each case, we included the set of ϕ/ψ angles occurring in the 1rx2 crystal structure as part of the clustering procedure. During the process, a user-defined cluster radius ensures that no member of a cluster is farther than the specified Euclidean distance from the cluster center. In all cases, this clustering radius was defined so as to generate distinct, well-separated groups. It was generally found that a range of cluster radii existed for which the number of clusters was invariant. It is these sets of clusters that were employed in order to evaluate the root-mean-square deviation (RMSD) between dihedral distributions.

To visualize the clustering data, we employed multidimensional scaling to project the clusters onto a two-dimensional plane. The projection was done to minimize the error (Φ) in intercluster distance in the reduced dimensional space (d_{ij}*) with respect to the RMSD in the full dihedral space (d_{ij}):

$$\Phi = \sum_{i=1}^{N} \sum_{j>i}^{N-i} (d_{ij} - (\alpha + \beta d_{ij}^*))^2 \quad (6)$$

where N is the number of clusters. The objective function Φ was minimized with respect to d_{ij}* and the parameters α and β. We found values of $\alpha = 20$ and $\beta = 10$ to provide satisfactory convergence. This is essentially the same approach employed by Karpen et al. in their application of clustering methods to characterize protein conformational states.[35]

2.4. Covariance Analysis. Solvent molecules were removed and the protein, ligand, and cofactor coordinates in every frame of each MD trajectory aligned on the basis of an RMS fit to heavy atom positions in order to compute the covariance matrix. The covariance of the spatial atom displacements, μ_{jk}, of atoms in each enzyme system is given by $\mu_{jk} = \langle (r_j - \langle r_j \rangle)(r_k - \langle r_k \rangle) \rangle$, where r_i represents the displacement of atom i. These covariance elements were employed to generate the normalized fluctuation covariance matrix M_{jk}, where $M_{jk} = \mu_{jk}/(\mu_{jj}\mu_{kk})^{1/2}$. The elements of M_{jk} are correlation coefficients for the spatial fluctuations of individual atoms. Covariance measurements provide a compact and efficient way to compare the coupling of fluctuations present in ensembles associated with each of the protein systems.

2.5. Quasiharmonic Analysis. The quasiharmonic (QH) model can be used to determine the principal components of fluctuations in molecular systems, in a manner analogous to normal-mode analysis.[36,37] To initiate this procedure, the covariance matrix was employed to compute QH modes using the VIBRAN module of CHARMM. We employed the modes resulting from the QH calculation to obtain entropy and classical free energy estimates using standard procedures.[38] Entropy values calculated in this manner are proportional to the configurational space explored by the system[39] and have been recently shown to be quite accurate.[40] Uncertainty estimates for the entropy values were obtained by dividing each PMF window into two equally sized segments and repeating the procedure for each. The deviation of each resulting value from the mean was employed to generate uncertainty estimates for the entropy computed for the entire window.

Fluctuations that decrease the hydride−acceptor distance are expected to reduce the hydride-transfer barrier height as well as its width. This proposal is related to the nearest attack conformer concept.[41] Configurations that preferentially decrease this distance will spend more time in the vicinity of the transition-state region. Thus, the hydride will be more readily conveyed over the transition-state barrier by thermal fluctuations or through the barrier via tunneling. Motion along similar coordinates has been implicated in increasing the efficacy of other enzyme-catalyzed hydride-transfer reactions.[42] Thus, we projected each QH mode onto the vector between the transferred hydride and the acceptor carbon in order to determine the degree of overlap between each mode and motion along this vector. The degree of overlap reveals the extent to which individual modes are coupled to motion along this vector. Using the average structure from each trajectory, atom C3 in the nicotinamide ring (see Figure 1) was translated along the hydride−acceptor vector. The resulting difference in the Cartesian coordinates was computed and projected onto each mode. We employed C3 as a proxy for the transferred hydride to ensure that the umbrella potentials present along the reaction coordinate did not mask the underlying motional tendencies present in each simulation. Atom C3 is adjacent to the donor carbon and is two covalent bonds away from the hydride. Motion of this atom along the hydride−acceptor vector reveals the intrinsic propensity for collective motion of the nicotinamide ring along this direction.

Table 2. Barriers to Hydride Transfer from DHFR Simulations

	$\Delta G_{MM/PM3}$[a]	$\Delta G_{MM/PM3/SVB}$[b]	ΔE_{MEP}[c]	λ[d]
WTLO	31.9	15.5	35.0	−0.01
WTHI	32.7	18.1	66.1	0.06
GSLO	31.3	15.0	32.2	0.07
GSHI	34.9	20.8	72.3	−0.08
GVLO	31.0	14.8	34.7	0.06
GVHI	37.7	19.6	59.5	−0.12

[a] Bare QM/MM potential. [b] QM/MM potential with SVB term included. [c] MEP hydride-transfer barriers from Thorpe and Brooks.[20] [d] Reaction coordinate value at transition state for PMF curves with SVB term added.

3. Results

3.1. Free Energy Barriers. Hydride-transfer barriers generated during the PMF simulations are presented in Table 2. PMFs that produce lower barriers without the SVB term also give lower barriers with inclusion of this term and vice versa. As we anticipated, addition of the SVB term allows trends in the magnitudes of barrier heights to remain relatively intact. Also presented in Table 2 are the energy barriers resulting from our prior MEP calculations carried out for the same initial configurations.[20] Snapshots that produced relatively high MEP barriers tend to produce relatively high PMF barriers and vice versa, indicating that the features of the enzyme system that modulate the hydride-transfer barrier in the MEP simulations also affect the barrier in the PMF simulations. PMF curves including the effects of the SVB term are displayed in Figure 2. These curves are displayed primarily for comparison with the work of Garcia-Viloca et al.[18] The appearance of the PMFs is similar to those presented by these authors. This is expected, given that the underlying Hamiltonian employed to generate these curves is similar to that used in their studies. Indeed, the lowest barriers we obtain are comparable to that obtained by these authors in their studies of the wild-type protein (16.1 kcal/mol).

In addition, the overall energies of reaction we obtain are comparable to the observations of these authors for all simulations except GSHI. In this case, there is a noticeably more favorable energy of reaction than observed for the other simulations. This is likely to be due to the fact that the SVB term was parametrized in order to reproduce the experimental energy of reaction and activation energy in only wild-type

(36) Brooks, C. L.; Karplus, M.; Pettitt, B. M. *Proteins: a theoretical perspective of dynamics, structure, and thermodynamics*; J. Wiley: New York, 1988.
(37) Case, D. A. In *Rigidity Theory and Applications*; Thorpe, M. F., Duxbury, P. M., Eds.; Kluwer Academic/Plenum Publishers: New York, 1999.
(38) Brooks, B. R.; Janećic, D.; Karplus, M. *J. Comput. Chem.* **1995**, *16*, 1522−1542.
(39) Karplus, M.; Kushick, J. N. *Macromolecules* **1981**, *14*, 325−332.
(40) Carlsson, J.; Aqvist, J. *J. Phys. Chem. B* **2005**, *109*, 6448−6456.
(41) Benkovic, S. J.; Bruice, T. *Biochemistry* **2000**, *39*, 6267−6274.
(42) Basner, J. E.; Schwartz, S. D. *J. Phys. Chem. B* **2004**, *108*, 444−451.

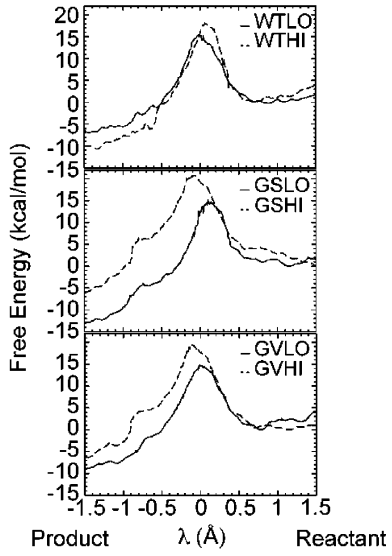

Figure 2. DHFR PMF curves incorporating the SVB correction term described in the text. The top, middle, and lower panels display results from the wild-type, G121S, and G121V simulations, respectively. In each panel the solids line represents LO simulations while the dotted line represents HI simulations (see section 2.1). The curves have been set to zero on the reactant side.

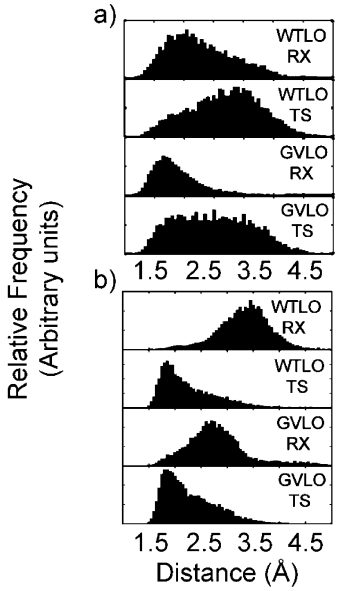

Figure 3. Hydrogen bonds that change with progress along the reaction coordinate and are associated with variations in the hydride-transfer barrier. Histograms of distance between NADPH ribose hydroxyl and the backbone carbonyl oxygen of (a) Ala 19 and (b) Arg 18 for simulations WTLO and GVHI (see section 2.1). Distributions for the reactant- (RX) and transition-state (TS) ensembles are displayed. The hydrogen bond to Ala 19 is observed preferentially in the RX, while the hydrogen bond to Arg 18 occurs preferentially in the TS, for simulations that generate lowered hydride-transfer barriers.

DHFR[18] and is thus unable to reproduce comparable energy values in regions of configuration space that differ from the wild-type configuration. Analysis of dihedral angle distributions (see section 3.2) demonstrates that the configurations observed during the GSHI simulation are quite different from those found in the wild-type protein. While the actual magnitude of the energy change may not correspond to experimentally determined values, the trends in energy differences are certainly meaningful when the different PMFs are compared. For consistency, we will limit further discussions to PMFs generated without considering the SVB term.

3.2. Characterization of Structural Interactions. Distributions of key structural interactions were found to differ in ensembles characterizing simulations with heightened or lowered hydride-transfer barriers, indicating that specific interactions are important for achieving a low hydride-transfer barrier. Several of these structural features are altered as the reaction proceeds from the reactant to transition states, suggesting that they are relevant to progress along the reaction coordinate. Examples include hydrogen bonds suggested to influence the hydride-transfer barrier in our previous work.[21] A case in point is the hydrogen bond between the carbonyl oxygen of alanine residue 19 (A19) and the second terminal hydroxyl of NADPH ribose (A19O−NH2T). In the wild-type and GVLO simulations this hydrogen bond is present in the reactant state but not in the transition state; this interaction is not formed in any of the other simulations. Conversely, the hydrogen-bonding interaction between the backbone carbonyl oxygen of asparagine 18 (N18) and the same NADPH hydroxyl group (N18O−NH2T) is absent from reactant states and present in transition states for all simulations except the GVHI and GSLO simulations. For the GVHI simulation this bond is present all along the reaction coordinate (though it is more prevalent in the transition state), while the GSLO simulation never exhibits this bond. Histograms of the distances between these hydrogen-bonding partners for the WTLO and GVLO simulations are displayed in Figure 3.

In our earlier studies we suggested that these interactions play a role in orienting the nicotinamide ring in a manner that alters hydride-transfer efficacy.[21] In those studies we implicated only A19O−NH2T in facilitating the hydride-transfer reaction. However, our present studies suggest that A19O−NH2T is required in order to generate favorable reactant complexes, while N18O−NH2T is necessary to generate transition states that favor the hydride-transfer reaction. Thus, it is only when both interactions are present at the appropriate locations along the reaction path that maximal reduction in the hydride-transfer barrier is obtained.

Other structural interactions display distinct distributions in simulations giving rise to low or high barriers but do not vary during the course of the reaction. Examples are provided by the hydrogen bond between the carboxyl oxygen of D122 and the backbone amine of E17 as well as the hydrogen bond between the backbone amine of D122 and the backbone carbonyl of G15 (Figure 4). These interactions are present only in the wild-type and GVLO simulations. The presence of these hydrogen bonds has also been noted by Swanwick et al.[43] Hammes-Schiffer and colleagues have implicated D122 and G15 as participants in a network of coupled fluctuations associated with the hydride-transfer process.[15] In addition, mutational analysis has demonstrated the importance of D122 to the catalytic ability of the enzyme.[44] The presence of these interactions as well as others noted in earlier work is supported by the correlated fluctuations of the corresponding atomic positions (Supporting Information).

Conformational fluctuations within proteins are determined to a large extent by the dihedral angles exhibited by the

(43) Swanwick, R. S.; Shrimpton, P. J.; Allemann, R. K. *Biochemistry* **2004**, *43*, 4119−4127.
(44) Miller, G. P.; Benkovic, S. J. *Biochemistry* **1998**, *37*, 6336−6342.

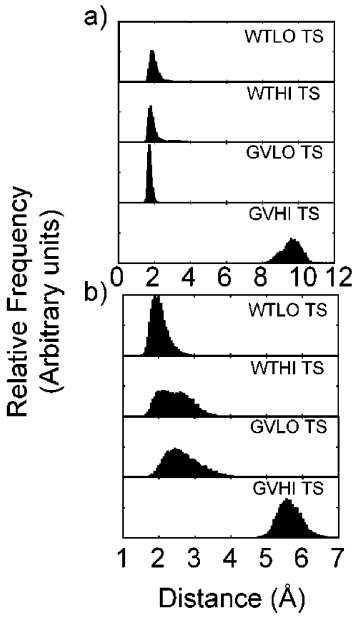

Figure 4. Hydrogen bonds that are unaltered with progress along the reaction coordinate and yet are associated with variations in the hydride-transfer barrier. Histograms of distance between the (a) side-chain carboxyl oxygen of D122 and the backbone amine of E17, and (b) backbone amine of D122 and the backbone carbonyl of G15 for wild-type and G121V simulations. Distributions for the transition-state (TS) ensembles are displayed. These hydrogen bonds occur preferentially in simulations that generate lowered hydride-transfer barriers.

polypeptide backbone. Consequently, noting the ϕ/ψ dihedral distribution of residues in a protein offers an efficient means to identify distinct regions of conformational space. Several studies indicate that the M20 loop plays an important role in determining hydride-transfer efficacy.[22,23,26,45,46] In particular, the closed conformation of this loop found in the 1rx2 crystal structure is thought to be more competent for hydride transfer than alternative conformations of the loop. Thus, we recorded the backbone dihedral distributions of residues 15−20 within the loop as well as of position 121 to assess the influence of loop conformations on the hydride-transfer barrier. We found that distinct ϕ/ψ values of residues within this loop are associated with lowered hydride-transfer barriers (see Table 3). Thus, conditions that engender lowered hydride-transfer barriers are associated with specific regions of conformational space. In addition, the equilibrium values of these dihedrals do not change significantly as the reaction proceeds, indicating that prior organization of the protein backbone has more of an impact on the barrier height than reorganization of backbone conformations in response to the reactive event.[8,13]

We quantified the similarity of different dihedral distributions by performing clustering analysis of the trajectories according to the ϕ/ψ distributions for these residues. Each simulation could be placed into a separate cluster. The dihedral RMSD between cluster centers is presented in Table 4, along with the corresponding values for the 1rx2 crystal structure. As schematically depicted in Figure 5, backbone dihedrals in simulations that generated low PMF barriers were generally more similar to each other than to those that generated high PMF barriers. Furthermore, the distributions of these dihedrals were usually more similar to those found in the M20 loop within the 1rx2 crystal structure (i.e., the closed form of the loop). Neither the GSLO nor the GSHI simulation demonstrates these patterns. The G121S protein exhibits a unique distribution of ϕ/ψ angles, indicating that it inhabits a region of conformational space that is very different from that occupied by the other two proteins. This may be an artifact of the original modeling of this mutant or a reflection of key differences arising from the glycine-to-serine substitution.

3.3. Covariance Analysis. We present cross-correlation plots for the C_α fluctuations occurring during simulations of the three proteins in Figure 6. Figure 6a displays reactant fluctuations, while Figure 6b displays fluctuations in the transition-state ensemble. Correlated fluctuations of the C_α atom within each residue are representative of the correlations between entire residues.

Several of the mobile loops within the enzyme (see Figure 1) participate in distinct patterns of correlation to other regions of the protein. Of particular note is the M20 loop, which engages in long-range coupling to the βF-βG loop (residues 116−132). There are many instances where specific correlated fluctuations are associated with a lowered hydride-transfer barrier (see Supporting Information). However, apart from these mobile loops, we do not observe regions of the protein that consistently exhibit long-range correlations. Wong et al. observed enhanced correlation of the region around residue 121 to the M20 loop in the transition state compared to the reactant state in their simulations of the wild-type[14] and G121S[47] proteins. These authors suggested that these correlations are associated with progress along the reaction coordinate. Some of the same observations are apparent in our simulations.

Overall, the extent of correlated motions is reduced in simulations, giving rise to lowered hydride-transfer barriers. In addition, the degree of correlation is generally reduced on going from the reactants to transition state. The patterns of correlation observed when comparing the reactant- and transition-state ensembles are very similar for each of the simulations that generated a low PMF barrier. In contrast, simulations that generated high PMF barriers exhibit patterns of correlation that differ more substantially as progress along the reaction coordinate is made.

3.4. Quasiharmonic Analysis. Table 5 contains entropy values calculated for the protein, DHF, and NADPH as a result of QH analysis. In addition, the classical free energy corresponding to the five modes with greatest overlap to fluctuation of the nicotinamide ring along the hydride−acceptor vector (see section 2.5) are displayed. Smaller entropy values are associated with fluctuations of decreased magnitude, which are consistent with the decreased correlations described in the previous section. While the numerical values of the entropy measurements are not necessarily significant, the differences between them are certainly relevant and are representative of actual entropy differences. Despite the uncertainty being appreciable in certain cases, the observed differences are often much larger. In general, simulations that produced reduced hydride-transfer barriers possess significantly less entropy than the high barrier simulations and exhibit less entropy at the transition state than in the

(45) Osborne, M. J.; Schnell, J.; Benkovic, S. J.; Dyson, H. J.; Wright, P. E. *Biochemistry* **2001**, *40*, 9846−9859.
(46) Schnell, J. R.; Dyson, H. J.; Wright, P. E. *Biochemistry* **2004**, *43*, 374−383.
(47) Wong, K. F.; Selzer, T.; Benkovic, S. J.; Hammes-Schiffer, S. *Proc. Natl. Acad. Sci. U.S.A.* **2005**, *102*, 6807−6812.

Table 3. Center of ϕ/ψ Dihedral Angle Distributions for Residues within the M20 Loop and Position 121 of DHFR

residue	1RX2	WTLO	WTHI	GVLO	GVHI	GSLO	GSHI
G15	−168/170	−150/165	−150/150	−135/150	−180/−150// −100/−150	−180/−180	165/−150
M16	−151/125	−150/−100	−140/75[a]	−145/100	−90/−80[a]	−90/−125[b]	−120/−50[b]
E17	49/42	50/50	50/175[a]	50/50	−100/−150	−100/−75[b]	−95/−125[b]
N18	64/33	75/0	70/−50[a]	75/0[b]	−120/−125	−110/−60	−100/−50[a]
A19	−155/169	−140/−150	−80/150[a]	−125/180[b]	−100/−75	−110/−180	−100/−180[a]
M20	−111/114	−125/150	−105/130	−105/140	−105/160	−80/150	−100/150[a]
121	−124/−171	180/180[b]	180/180	−110/−150	−100/110	−155/150	−155/150

[a] More compact distribution in reactant state. [b] More compact distribution in transition state. The // symbol demarcates two separate clusters. The first column contains values found in the 1rx2 crystal structure.

Table 4. Intercluster Dihedral RMSD (in Degrees) from DHFR Simulations[a]

protein	WTLO	WTHI	GVLO	GVHI	GSLO	GSHI
1RX2	19.7	40.4	26.0	103.5	90.3	93.6
WTLO	–	33.2	47.4	78.4	101.7	92.4
WTHI		–	25.2	91.6	105.1	98.4
GVLO			–	101.9	87.3	90.3
GVHI				–	41.2	52.0
GSLO					–	24.0
GSHI						–

[a] For clarity, only the upper diagonal of the symmetric RMSD matrix is shown.

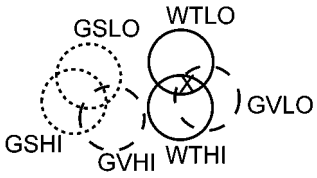

Figure 5. Schematic diagram displaying similarity of reactant-state ensembles based on clustering of backbone ϕ/ψ distributions. Trajectories were clustered on the basis of the dihedrals of residues 15−20 and 121 as described in section 2.3. The RMSD between cluster centers (Table 4) was then projected onto two dimensions using eq 6. Each trajectory generated individual clusters (labeled circles). The distance between the centers of the circles represents the RMSD between cluster centers. Simulations that exhibit lowered hydride-transfer barriers tend to exhibit dihedral angles that are more similar to the pattern of dihedrals found in the 1rx2 crystal structure (X in the plot).

reactant state. These simulations also exhibit reduced classical free energy for the five modes most strongly coupled to motion along the hydride−acceptor vector in the transition-state region. This indicates that the eigenvalues (frequencies) of modes most strongly coupled to motion in this direction tend to decrease. Thus, the amplitude of motion along this direction increases in these simulations. Larger amplitude motion along this vector is likely to be more effective in facilitating hydride transfer. Chemical reactions can involve fluctuations along a number of different coordinates.[48] As a result, motion along other coordinates can potentially impact the hydride-transfer reaction. However, such fluctuations are only relevant to the differences in the hydride-transfer barriers we observe if they differ in simulations giving rise to altered barrier heights. Projection of the QH modes onto alternate vectors did not display any such correlations to the hydride-transfer barrier.

4. Discussion

4.1. Mutations at Glycine 121 Perturb Conformational Substates in DHFR. Distinct structural interactions exist within wild-type and mutant DHFR which do not interconvert on the

(48) Warshel, A.; Parson, W. W. *Q. Rev. Biophys.* **2001**, *34*, 563−679.

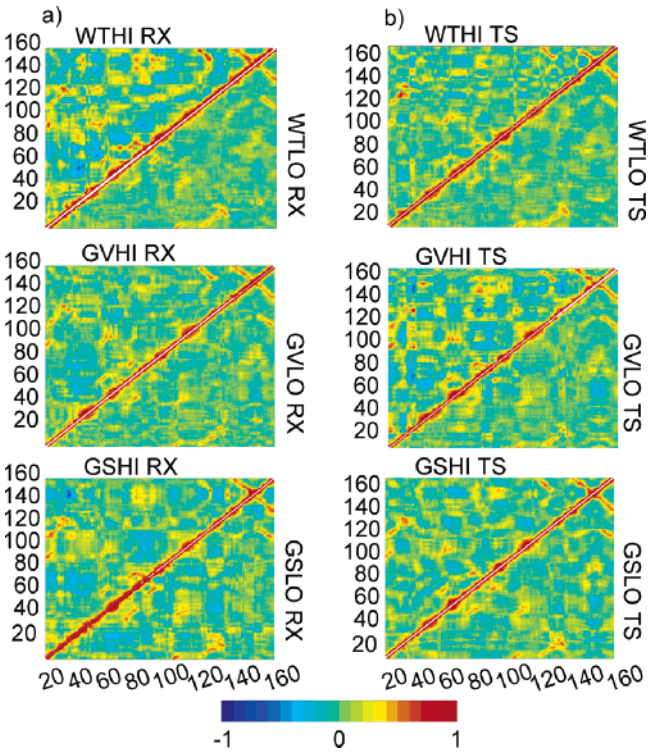

Figure 6. Correlated fluctuations for C_α positions in (a) reactant-state ensembles and (b) transition-state ensembles for DHFR simulations. The top, middle, and bottom panels of each figure correspond to the wild-type, G121V, and G121S proteins, respectively. In each panel the upper diagonal of each plot contains the correlations present in the simulations originating from snapshots that generated a large MEP barrier in our previous work.[20] The lower diagonal contains correlations occurring in simulations originating from snapshots with a small MEP barrier. The color scale presented in the bar ranges from blue for perfect anticorrelation to red for perfect positive correlation. Numbers denote residue positions along the sequence.

time scale of the simulations. Their long-lived nature indicates they are components of conformational substates in the protein. This observation is consistent with our previous suggestion that the structural properties of DHFR are altered as a result of mutations at glycine 121[21] and is supported by the results of other recent studies. Experimental and computational studies by Swanwick et al. demonstrate that the G121V mutant exhibits altered structural characteristics relative to the wild-type protein.[43] Theoretical investigations by Wong et al. indicate that the G121S mutation perturbs the equilibrium ensemble of configurations present in the protein.[47] NMR studies by Venkitakrishnan et al. reveal that the G121V mutation interferes with the structure and motion of the M20 loop in a manner consistent with the reduced hydride-transfer efficacy exhibited by this mutant.[23]

Table 5. Properties Computed via Quasiharmonic Analysis

		total entropy (kcal/mol·K)	free energy of high overlap modes[a] (kcal/mol)
WTLO	RX	6.361 (0.015)	1.234
	TS	6.322 (0.002)	2.68
WTHI	RX	6.405 (0.025)	2.62
	TS	6.414 (0.008)	3.47
GVLO	RX	6.351 (0.021)	1.96
	TS	6.334 (0.008)	1.87
GVHI	RX	6.433 (0.009)	6.63
	TS	6.429 (0.001)	3.40
GSLO	RX	6.419 (0.034)	6.84
	TS	6.383 (0.014)	3.00
GSHI	RX	6.419 (0.011)	5.18
	TS	6.417 (0.023)	7.29

[a] Combined classical free energy of the five modes with greatest overlap to motion along the hydride−acceptor vector as described in section 2.5. RX and TS denote reactant- and transition-state ensembles, respectively. Uncertainty estimates for entropy values are given in parentheses.

One could consider that DHFR mutations of glycine 121 are allosteric effectors, altering the structure of the enzyme at distant locations. While allostery is usually applied to intermolecular interactions, Gunasekaran et al. have suggested that it may also be applied to mutational changes.[49] The potential for this phenomenon in DHFR has been demonstrated by Pan et al., who showed that structural properties of different regions of the protein are energetically coupled.[50]

4.2. Substates Modulate the Barrier to Hydride Transfer. Each substate has the potential to produce a unique hydride-transfer barrier. An important point to note is that the microscopic barrier to hydride transfer is not an intrinsic property of a particular DHFR protein, as specific substates from any of the DHFR variants investigated in this study can give rise to low or high barriers. The experimentally measured macroscopic hydride-transfer barrier incorporates contributions of all (individual) microscopic hydride-transfer barriers and reflects differences in the characteristics and distributions of the substates. Backbone conformations of the M20 loop are important components of conformational substates within DHFR. As noted previously, the closed conformation of the M20 loop is thought to be most competent for hydride transfer.[26,45,46] Consistent with this proposal, clustering analyses of our data confirm that simulations with conformations more similar to the closed form generally exhibit lowered hydride-transfer barriers (Table 4 and Figure 5).

The role of substates in modulating protein function is not unprecedented. The term was employed by Frauenfelder and colleagues in discussions of myoglobin.[25] This phenomenon has been verified by Yang et al., who observed time-dependent fluctuations in the reactivity of flavin reductase during single-molecule experiments.[51] Zhang et al. made similar observations in their studies of acetylcholinesterase.[52] These authors employed MEP calculations to probe the reactive event in configurations taken from MD simulations and obtained a number of distinct reaction barriers for these configurations, in analogy to our earlier findings on DHFR.[20] Glennon and colleagues also noted that different configurations of the Ras protein generated altered free energy barriers.[53]

A particularly striking example is provided by studies by Garcia-Viloca et al. pertaining to the enzymes acyl-CoA dehydrogenase and xylose isomerase.[54] These authors discovered that initial configurations originating from different crystal structures of these proteins resulted in reaction profiles with different characteristics, including distinct barrier heights. The computed reaction barriers differed by up to 17 kcal/mol and energies of reaction by up to 22 kcal/mol. These free energy profiles were deduced via QM/MM PMF simulations, as in the present study. Each crystal structure represents the average of a thermally accessible ensemble that necessarily occupies a distinct basin on the potential energy hypersurface of the protein. Thus, each crystal structure potentially represents a different substate. The findings of these authors demonstrate the marked effects that substates can have on enzymatic reactivity.

4.3. Specific Patterns of Protein Fluctuations Characterize Each Substate. In addition to distinct structural ensembles, we observe that DHFR fluctuations differ with respect to the hydride-transfer barrier height. In particular, specific vibrational modes anticipated to decrease the hydride-transfer barrier occur with larger amplitude in the transition states of low-barrier simulations. This suggests that the corresponding protein environments exhibit motions that promote hydride transfer to a greater extent in these simulations.

At the same time, correlated fluctuations in most parts of the protein decrease in simulations that exhibit reduced barrier heights. Numerous studies suggest that correlated motions involving distant regions of DHFR impact hydride-transfer proficiency.[12−15,19,47] As noted by several of these authors,[15,47] such correlations are not necessarily causative and may simply be the results of altered structural interactions present in the proteins. Our current observations suggest that the majority of correlated motions observed for DHFR do not have a direct role in facilitating hydride transfer. However, these fluctuations may serve other purposes. For example, they may facilitate transitions into appropriate substates. The increased magnitude of fluctuations observed for the WTHI simulation in comparison with WTLO may represent effective realizations of this reorganization process (see section 4.4). One impact of mutations could be to make these fluctuations less effective at populating substates that are conducive to hydride transfer.

Enzymes have evolved to facilitate the reactions they catalyze through specific interactions. Consequently, substates that exhibit enhanced reactivity likely represent relatively deep basins on the energy landscape, subject to diminished extraneous (i.e. nonproductive) fluctuations. Using ^{15}N relaxation dispersion measurements, McElheny et al. computed a significant (∼13 kcal/mol·K) increase in entropy as DHFR is converted from the closed to the nonproductive occluded form of the enzyme.[55] While this conformational change is of larger scale than differences among the conformations present in our simulations, these findings are consistent with our observations that configurations of the protein more competent for hydride transfer generally possess less entropy. In such cases, the available

(49) Gunasekaran, K.; Ma, B.; Nussinov, R. *Proteins* **2004**, *57*, 433−443.
(50) Pan, H.; Lee, J. C.; Hilser, V. J. *Proc. Natl. Acad. Sci. U.S.A.* **2000**, *97*, 12020−12025.
(51) Yang, H.; Luo, G.; Karnchanaphanurach, P.; Louie, T. M.; Rech, I.; Cova, S.; Xun, L.; Xie, X. S. *Science* **2003**, *302*, 262−266.
(52) Zhang, Y.; Kua, J.; McCammon, J. A. *J. Phys. Chem. B* **2003**, *107*, 4459−4463.
(53) Glennon, T. M.; Villa, J.; Warshel, A. *Biochemistry* **2000**, *39*, 9641−9651.
(54) Garcia-Viloca, M.; Poulsen, T. D.; Truhlar, D. G.; Gao, J. *Protein Sci.* **2004**, *13*, 2341−2354.
(55) McElheny, D.; Schnell, J. R.; Lansing, J. C.; Dyson, H. J.; Wright, P. E. *Proc. Natl. Acad. Sci. U.S.A.* **2005**, *102*, 5032−5037.

thermal energy in the system may be preferentially funneled into vibrational modes that favor reactivity, leading to a reduction in overall fluctuations but an enhancement of specific barrier-reducing motions.[56] This could occur, for example, if the free energy required to populate these modes is reduced in low-barrier configurations (i.e., the modes have higher Boltzmann weights). Some authors have used the term "dynamical effects" to imply the coherent non-Boltzmann funneling of energy into particular coordinates.[48,57] The effect we observe is not "dynamical" in this respect, as Boltzmann weighting still applies to the vibrational modes identified. Nonetheless, the effects are dynamic in the sense that the redistribution of thermodynamic weights associated with these modes modifies the protein fluctuations which are observed.

4.4. Protein Reorganization Influences Hydride-Transfer Proficiency. The PMF hydride-transfer barriers agree in a qualitative sense with the trends obtained from MEP calculations subject to the same initial conditions. This indicates that the PMF simulations sample regions of conformational space similar to those probed by the MEP calculations. Thus, as we had previously suggested,[20] the structural ensembles impacting hydride transfer are very similar to those observed in equilibrium simulations which did not explicitly probe the reactive event.

The main difference between the MEP and PMF approaches is that while the MEP calculations employed primarily frozen environmental (solvent + protein) coordinates, the PMF simulations incorporate no restraints apart from umbrella potentials along the reaction coordinate. Consequently, the PMF simulations allow more reorganization of the environment to occur in response to hydride translocation. The larger reduction in the barrier that accompanies adoption of a PMF treatment for the WTHI simulation compared to the GVHI and GSHI simulations may indicate that wild-type DHFR is able to reorganize in response to hydride translocation much more effectively than the mutant proteins. All the simulations were carried out at the same temperature. Thus, the (thermal) energy available to available to elicit such reorganization is the same in each case. The time scale for environment reorganization is related to the energy barrier for this process.[58] Given that the different simulations are of comparable time scales, the more comprehensive reorganization observed in the WTHI simulation compared to that in the GSHI and GVHI simulations suggests that the energy barrier associated with this structural rearrangement is reduced in the wild-type protein.

Since backbone ϕ/ψ angles do not vary significantly during the simulations, reorganization of the protein occurs primarily with respect to side-chain conformations. The ϕ/ψ distribution observed in the WTHI protein is already fairly similar to that found in the WTLO simulation (Tables 3 and 4). Thus, the reorganization of WTHI to facilitate hydride transfer may require significant changes only in side-chain conformations. This observation may be relevant to the decreased hydride-transfer efficacies in the mutant enzymes. As we suggested in a previous study,[21] the backbone ϕ/ψ angles of the wild-type protein may predominantly occupy regions of conformational space that are conducive to hydride transfer, while the mutant proteins visit alternative conformations. Reorganization from these suboptimal backbone conformations may contribute to the free energy barrier to hydride transfer in the mutant proteins.

4.5. The Presence of Substates Highlights Limitations of PMF Approaches for Enzymatic Reactions. It is possible for PMF-based approaches to generate realistic free energy differences in enzyme systems.[53] In principle, a PMF is valid in the limit of infinite sampling; in practice, only a restricted region of conformational space is sampled in such calculations. This issue was noted in our previous work[21] as well as by Garcia-Viloca et al.[54] As a result, PMF-based approaches are likely to work best for proteins that occupy a limited number of configurations. In the case of DHFR, large-scale fluctuations occur [55,59−61] that involve traversal of various conformational substates. Because each PMF presented in this study characterizes a relatively limited region of configuration space (i.e., only within a given substate), the resulting free energy barriers do not necessarily reproduce the experimentally measured differences in hydride-transfer barriers among the three proteins. Based on the hydride-transfer reaction rate, the activation free energy difference between wild-type DHFR and G121V is approximately 3 kcal/mol ($\Delta\Delta F^{\ddagger} = 3$ kcal/mol); the corresponding value for G121S is $\Delta\Delta F^{\ddagger} = 1$ or 2.4 kcal/mol, depending on the particular set of experiments considered.[10,11,15] To reproduce these trends, an averaging procedure is required that takes transitions between substates into account. Such averaging could be accomplished simply by performing a longer PMF simulation. However, conformational transitions in proteins are relatively rare (on the order of nanoseconds or longer) because they are linked to changes in backbone dihedrals.[62] Evidence for the presence of substates in DHFR indicates that the 10 ns of MD from which our initial configurations were taken is sufficient for some transitions between these substates to occur; a recent PMF study of DHFR has been carried out with sampling on a comparable time scale.[14] However, it is possible that a PMF simulation for hydride transfer in DHFR would not provide a converged free energy unless it approaches a length of several tens of nanoseconds.

Unfortunately, carrying out PMF calculations with such extensive sampling tends to be prohibitively expensive from a computational standpoint. We suggest that a limited number of short PMFs can be run and averaged in order to generate a well-converged free energy barrier. The initial configurations for these simulations could be snapshots from conventional equilibrium MD simulations. By considering an equilibrium distribution of reactant states, switching between substates is fully taken into account, as all substates will occur with their correct Boltzmann weight.[63] As we noted in our previous study,[20] this method is essentially a free energy perturbation (FEP) approach, where the free energy difference between reactant and transition states is evaluated at the equilibrium distribution of reactant states. Several authors have demonstrated that the exponential connection formula employed for FEP calculations can be applied to treat either equilibrium or nonequilibrium perturba-

(56) Antoniou, D.; Caratzoulas, S.; Kalyanaraman, C.; Mincer, J. S.; Schwartz, S. D. *Eur. J. Biochem.* **2002**, *269*, 3103−3112.
(57) Villa, J.; Warshel, A. *J. Phys. Chem. B* **2001**, *105*, 7887−7907.
(58) Steinfeld, J. I.; Francisco, J. S.; Hase, W. L. *Chemical kinetics and dynamics*; Prentice Hall: Upper Saddle River, NJ, 1989; pp 390−404.
(59) Falzone, C. J.; Wright, P. E.; Benkovic, S. J. *Biochemistry* **1994**, *33*, 439−442.
(60) Miller, G. P.; Benkovic, S. J. *Biochemistry* **1998**, *37*, 6327−6335.
(61) Miller, G. P.; Benkovic, S. J. *Chem. Biol.* **1998**, *5*, R105−113.
(62) Braxenthaler, M.; Unger, R.; Auerbach, D.; Given, J. A.; Moult, J. *Proteins* **1997**, *29*, 417−425.
(63) Tobias, D. J.; Brooks, C. L.; Fleischman, S. H. *Chem. Phys. Lett.* **1989**, *156*, 256−260.

tions.[64−66] A conventional PMF simulation embodies the former approach, while a simple one-step FEP calculation embodies the latter. Our previous MEP approach represents a nonequilibrium work measurement[66] between these two extremes. Luo and Bruice have since successfully applied this approach in studies of the enzyme horse liver alcohol dehydrogenase.[67] It should be possible to also apply similar approaches to average a number of PMF simulations in order to obtain a well-converged free energy barrier. Recent work by Shirts and Pande evaluates a number of such averaging procedures;[68] such methods are likely to prove useful in combining the contributions of different enzyme substates.

Apart from the computational expense, another disadvantage of simply carrying out a lengthy PMF calculation is the difficulty of identifying transitions between substates with such an approach. Examining a distribution of barriers (via either MEP or PMF calculations) rapidly informs us about the location and number of basins in the energy landscape, allowing us to characterize the properties of these substates. In doing so, we are able to identify the determinants of barrier height in a straightforward manner. Fluctuations that generate lowered barriers are well represented in a typical PMF simulation because the lowest barrier configurations make the greatest contribution to the free energy barrier. As we strive to understand the factors that modulate protein function, it may also be useful to characterize high-barrier configurations with the goal of understanding their origin. This approach is also amenable to parallelization, as simulations to characterize each substate can be performed independently, greatly reducing the computational cost compared to that of a single, long PMF simulation.

5. Concluding Remarks

Protein dynamics involves movement through a high-dimensional space. This space can include a number of local minima that exhibit distinct structural properties. The presence of long-lived basins (i.e. substates) in this energy landscape should not be overlooked when considering the structure and function of these molecules. Accounting for the presence of substates is likely to be necessary for any enzyme flexible enough to undergo conformational transitions. Our results demonstrate that such substates differentially impact the hydride-transfer reaction in DHFR and indicate that the long-range effects of mutations at position 121 are mediated by redistribution of conformational substates present in the protein.

In previous work we suggested that protein dynamics was not essential to understand effects of mutation on the hydride-transfer barrier in DHFR. Our current observations are consistent with this proposal, as the energetic and structural trends we obtain by allowing unhindered dynamical evolution of the system during PMF simulations are similar to those observed by employing immobile equilibrium distributions of protein conformations. These findings support a role for preorganization in catalysis carried out by DHFR, with particular substates providing environments that are preconfigured to favor the hydride-transfer reaction. The importance of a preconfigured enzyme environment is a long-standing concept[69] that has been implicated in the function of other enzyme systems.[41,57,70,71]

However, our present work reveals that these conformational distributions are also associated with specific motional tendencies that correlate to the hydride-transfer barrier height. Collective motions expected to facilitate hydride transfer exhibit larger amplitudes in the transition states of simulations, giving rise to lowered hydride-transfer barriers. While arguments have been made that coherent protein motions do not contribute significantly to catalysis,[57] our observations leave open the possibility that specific protein motions play a role in determining enzymatic reactivity in DHFR. Such suggestions have been made by previous authors in the context of other enzyme systems.[42,56,72]

The dynamical evolution of a complex system and the equilibrium distribution of configurations present in that system are inextricably linked. It is difficult to determine which of these two factors plays the primary role. However, we note that the initial conditions for these simulations were originally identified via a procedure that removed all information regarding the inherent dynamics present.[20] Consequently, currently observed differences in the dynamics must result only from differences in the configurations employed in each case. This suggests that the configurations present induce the dynamical changes observed, rather than the converse.

Finally, we note that employing a single free energy barrier generated via a PMF approach in order to characterize an enzyme-catalyzed reaction may be problematic. This procedure does not provide information with respect to the number of substates and the fluctuations that occur within each. Furthermore, such approaches tend to sample a limited region of configurational space. Conformational transitions in proteins are governed by processes that occur on the nanosecond time scale, making PMF generation difficult when it involves large conformational changes. In the case of DHFR, significant changes in the structure of the mobile M20 loop have been shown to be relevant to hydride-transfer efficacy, suggesting that conformational switching will have an important impact on the barrier to hydride transfer in this enzyme.

Acknowledgment. We thank Professor Jiali Gao for helpful discussions. Financial support from the National Institutes of Health (GM 56879 and GM 37554) is acknowledged.

Supporting Information Available: Covariance values computed for pairs of atoms suggested to impact the hydride-transfer barrier in DHFR. This material is available free of charge via the Internet at http://pubs.acs.org.

JA053558L

(64) Jarzynski, C. *Phys. Rev. Lett.* **1997**, *78*, 2690−2693.
(65) Jarzynski, C. *Phys. Rev. E* **1997**, *56*, 5018−5035.
(66) Wu, D.; Kofke, D. A. *J. Chem. Phys.* **2004**, *121*, 8742−8747.
(67) Luo, J.; Bruice, T. C. *Proc. Natl. Acad. Sci. U.S.A.* **2004**, *101*, 13152−13156.
(68) Shirts, M. R.; Pande, V. S. *J. Chem. Phys.* **2005**, *122*, 144107.
(69) Warshel, A. *Proc. Natl. Acad. Sci. U.S.A.* **1978**, *75*, 5250−5254.
(70) Young, L.; Post, C. B. *Biochemistry* **1996**, *35*, 15129−15133.
(71) Olsson, M. H.; Warshel, A. *J. Am. Chem. Soc.* **2004**, *126*, 15167−15179.
(72) Williams, G. S. B.; Hossain, A. M.; Kranbuehl, D. E.; Bagdassarian, C. K. *J. Phys. Chem. B* **2003**, *107*, 12527−12533.